Hindawi
Shock and Vibration
Volume 2019, Article ID 6981482, 14 pages
https://doi.org/10.1155/2019/6981482

*Research Article*

# Thermal EHL Characteristics Investigation on Axle Box Bearings of Railway Vehicle Based on Slicing Method

**Junzhou Huo**,[1,2] **Jianjun Zhou**,[1] **Tao Li**,[2] **Zhichao Meng**,[2] **and Wei Sun**[2]

[1]*State Key Laboratory of Shield Machine and Boring Technology, Zhengzhou 450001, China*
[2]*School of Mechanical Engineering, Dalian University of Technology, Dalian 116024, China*

Correspondence should be addressed to Tao Li; litao221@mail.dlut.edu.cn

Received 18 December 2018; Revised 19 February 2019; Accepted 3 March 2019; Published 2 April 2019

Academic Editor: Giuseppe Ruta



Lubrication failures of axle box bearings can lead to accidents, such as bearing burnout and hot axle cutting. Presently, the modeling of the vehicle-track system dynamics rarely considers the nonlinear contact load of axle box bearings, and this leads to imperfection in the vehicle-track system dynamics calculation. And then, the load distribution and lubrication characteristics of axle box bearings are difficult to obtain. Therefore, in this paper, we fully consider the time-varying nonlinear contact load of bearings and track irregularity in establishing the bearing-wheel-rail system coupling-dynamics model. The dynamic response of axle box bearings is obtained by taking the vertical, strong impact-time-varying load on the carrying saddles as the external excitation. The load-balance equation of dynamic pressure lubrication is then obtained, according to the slicing method of bearing rollers. Finally, the elastohydrodynamic lubrication (EHL) model of axle box bearings is established considering thermal and scale effects. The results show that the central film thickness under thermal EHL was decreased by 13.61% compared with that under isothermal EHL. As the velocity of the contact pair increases, the thickness difference between thermal and isothermal EHL became larger. Thermal effects should be considered in the EHL model, in order to truly reflect the characteristics of EHL under a high speed.

## 1. Introduction

The axle box bearing of a vehicle-track system is the pivotal components of a vehicle bogie, which bears a variety of complicated stochastic loads between the bogie and the track. The service life and reliability of axle box bearings can influence the vehicle safety. However, improper lubrication can lead to serious accidents such as hot axle cutting. A good bearing lubrication state will largely improve the bearing service life and performance.

A number of researches have been carried out on the design of vehicle/track systems [1–9]. Researchers have been mainly giving attention on the wheel-bogie system and overall vehicle system characteristics, so they regard axle box bearings and wheelsets as a whole [5–9]. In order to study the lubrication characteristics of axle box bearings, it is necessary to obtain the time-load history of bearings by establishing the bearing-wheel-rail system-coupled dynamics model. In recent years, studies of EHL have mainly focused on theoretical model research and testing technology. Some scholars have studied on lubrication characteristics of high-speed rotating machines in theory or experimental techniques [10, 11]. Yang and Wen [12] proposed a generalized Reynolds equation for a non-Newtonian thermal EHL. Rong-Tsong and Chao-Ho [13] proposed the fast and accurate solution of the coupled equations of thermal EHL. Habchi and Issa [14, 15] obtained the coupled strategies and solution for finite-element modeling of thermal EHL problems. Hili et al. [16] studied the effect of the speed and temperature on the film thickness, based on the thermal EHL experimental investigation. On the basis of the Navier-Stokes equation, the thermal EHL model of finite contact lines was established by Bruyere et al. [17], considering the highly non-Newtonian behavior and thermal effects of lubricants. Mihailidis et al. [18] proposed a new thermal EHL model of finite line contacts, taking into account the external profile of rollers, non-Newtonian properties, and starved lubrication characteristics. The edge-contact effect of finite contact lines on thermal EHL was studied by Najjari and Guilbault [19]. Wu et al. [20] proposed a thermal EHL model of an optimized cam-tappet pair in smooth contact and

mainly studied the effect of temperature on the THL of the cam-tappet pair. Liu et al. [21, 22] mainly studied load and velocity effects on the thermal EHL performance of a helical gear pair. At present, most scholars [17–22] have studied thermal EHL models of finite line contacts, which consist of two cylindrical surfaces, the synthetic curvature of which is constant, so the EHL model is not needed to consider the scale effect of contact pairs.

In short, while scholars have made strides in wheel-rail dynamics, they have ignored the influence of nonlinear contact forces on the bearing system. Such a simplification of the model affects the correctness of calculations of the vehicle-track dynamics, and thus, the load distribution of the bearing cannot be accurately obtained. It is thus difficult to obtain the boundary-load conditions for researching axle box bearings lubrication characteristics. In recent years, scholars have conducted deep studies of the thermal EHL of finite contact lines and have considered many key factors, such as the non-Newtonian, scale, and thermal effects of lubricants in the theoretical model [17–22]. They have not, however, established a thermal EHL model of tapered roller bearings, based on the scale effect between the roller and ring raceway. At the same time, to our knowledge, literature on the lubrication characteristics of vehicle axle box bearings has not yet appeared.

This study aims to first establish the bearing-wheel-rail system-coupled dynamics model and then obtain the dynamic response of axle box bearings according to the strong impact-time-varying load on the carrying saddles. The thermal EHL model of axle box bearings is then established based on the bearing load and EHL theory. Additionally, the scale effect of tapered roller bearings is taken into account, and the slicing method is applied to establish the load-balance equation of dynamic pressure lubrication. The three-dimensional complex problem is transformed into the line-contact problem of thermal EHL, and then the numerical solution is obtained using the multigrid method. Finally, the pressure and thickness distribution law of lubricating grease is studied, and the lubrication characteristics of the bearing are analyzed. Thus, this study has a major theory value and engineering significance to research intensively and design the lubrication system for axle box bearings.

## 2. Materials and Methods

*2.1. Coupled Dynamics Model of Wheelset-Rail System.* The wheelset-rail system mainly consists of the axle box, axle box bearings, wheel axle, wheels, and rails. The bearing outer ring and the adapter are connected under an interference fit and so do the inner rings and the wheelset axle. The wheel is mounted on both sides of the axle. The wheelset directly contacts the rails.

The bearing saddle is subjected to vertical excitation to the bearing, and the bearing nonlinear load is transmitted to the wheelset. Finally, the wheelset transfers the load to the track, while the track irregularity affects the vehicle wheelset. On the basis of working principle, the force distribution of the bearing-wheel-rail system [23] is shown in Figure 1. $k_{cy}$ and $c_{cy}$ are the equivalent radial-stiffness and radial-damping of adapters; $F_{v1}(t)$ and $F_{v2}(t)$ are the dynamic excitation on the right adapter and left adapter, and $F_{r1}$ and $F_{r2}$ are the contact forces of the axle box bearings.

*2.1.1. Modeling of Adapter-Bearing System.* Based on the lumped parameter method, the bearing-coupled characteristic is analyzed. The adapter, the bearing outer ring, and the bearing inner ring are regarded as a mass, respectively. The force diagram of the wheel-rail system is shown in Figure 1. The dynamics differential equation is obtained:

$$\begin{cases} m_c\ddot{z}_{c1} + k_{cy}(z_{c1} - z_{b1}) + c_{cy}(\dot{z}_{c1} - \dot{z}_{b1}) = F_{V_1}(t) + m_c g, \\ m_b\ddot{z}_{b1} - k_{cy}(z_{c1} - z_{b1}) - c_{cy}(\dot{z}_{c1} - \dot{z}_{b1}) = m_b g - F_{r1}, \\ m_c\ddot{z}_{c2} + k_{cy}(z_{c2} - z_{b2}) + c_{cy}(\dot{z}_{c2} - \dot{z}_{b2}) = F_{V_2}(t) + m_c g, \\ m_b\ddot{z}_{b2} - k_{cy}(z_{c2} - z_{b2}) - c_{cy}(\dot{z}_{c2} - \dot{z}_{b2}) = m_b g - F_{r2}, \end{cases} \tag{1}$$

where $m_c$ and $m_b$ are the equivalent mass of the left adapter and bearing inner ring, $z_{c1}$ and $z_{b1}$ are the vibration displacements of the left adapter and left bearing, and $z_{c2}$ and $z_{b2}$ are the vibration displacements of the right adapter and right bearing.

The vibration performance of a bearing is the combined effect of its structural parameters and internal geometric motion under external loads [24, 25]. In this paper, the rigid-ring hypothesis is adopted, in which the outer ring is considered a mass point and the bearing rolls and inner ring are considered another mass point.

A schematic diagram of the bearing force is shown in Figure 2. $\delta_r$ is the radial displacement of the bearing outer ring, and $\delta_{wn}$ is the roller normal displacement at $\Phi_w$. $\alpha_i$, $\alpha_e$, and $\alpha_f$ are the contact angle, the roller cone angle, and the flange angle, respectively.

The radial balance equation of two row tapered roller bearings [23]:

$$F_r = \sum_{i=1}^{2}\sum_{w=1}^{Z} K\delta_{iwn}^{1.11} H(\delta_{iwn})\cos\alpha_e \cos\phi_{iw}, \tag{2}$$

where $K$ is the contact stiffness of roller and raceway, $H$ is the function of the judging roller contact state, $i$ is the number of the bearing row, and $Z$ is the number of bearing with single row rollers.

*2.1.2. Wheel-Rail Dynamic Model.* Since the rail and wheel are elastic bodies, the interaction between each can be described by the classical Hertz nonlinear contact theory. $N_{Ly}$ and $N_{Ry}$, which are the normal contact forces of wheel-rail systems, will be obtained by contact theory [7]:

$$\begin{cases} N_{Ly}(t) = \left[\frac{1}{G}\delta(Z_L(t))\right]^{3/2}, \\ \\ N_{Ry}(t) = \left[\frac{1}{G}\delta(Z_R(t))\right]^{3/2}, \end{cases} \tag{3}$$

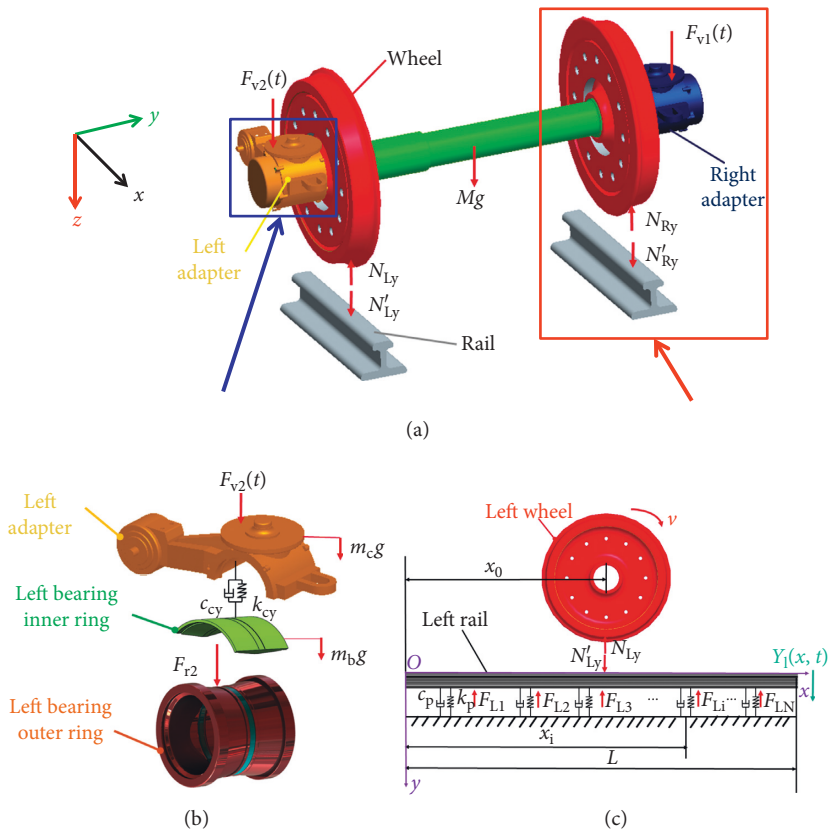


FIGURE 1: General force diagram of the dynamic system: (a) force diagram of the bearing-wheel-rail system; (b) force diagram of the adapter-bearing system; (c) force diagram of the wheel-rail system.

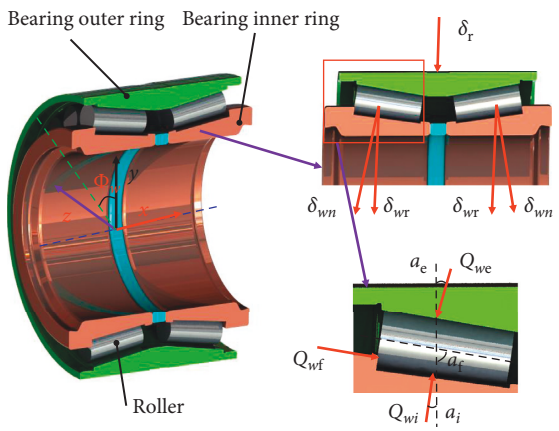


FIGURE 2: Force diagram of the axle box bearing.

where $G$ is the wheel-rail contact coefficient and $\delta(Z_L(t))$ and $\delta(Z_R(t))$ are the elastic compression of the left- and right-wheel-rail systems.

Based on the long sleeper buried-type ballastless track system, in this paper, we use the Euler beam model [26], the force model of which is shown in Figure 1(c), where $N_{Ly}$ and $N'_{Ly}$ are the left wheel-rail contact force and contact reaction, respectively. The speed of wheelset is $v$, $F_{Li}$ $(i = 1 - N)$ is the reacting force on the sleepers, and $N$ is the number of resilient pads on the continuous slab of concrete. $Y_1(x,t)$ is the displacement function of track's vertical vibration. $k_p$ and $c_p$ are the stiffness and damping of the track plate, respectively.

### 2.2. Thermal EHL Model of Axle Box Bearings

*2.2.1. Contact-Pair Parameters.* Assuming that the rollers and raceway undergo continuous pure rolling, the equivalent velocity and integrated curvatures of the contact pair between roller and raceway can be obtained as follows:

$$\begin{cases} R_i = \dfrac{d(1-\lambda)}{2}, \\ R_o = \dfrac{d(1-\lambda)}{2}, \\ U = \dfrac{\pi n d\left(1-\lambda^2\right)}{120\lambda}, \end{cases} \tag{4}$$

where $n$ is the speed of the bearing inner ring; $d$ is the diameter of an arbitrary section of the roller; $\lambda = 2\,d/R_1 + R_2$, where $R_1$ is the radius of the inner raceway and $R_2$ is that of the outer raceway; $R_i$ is the integrated curvatures of inner raceway; and $R_o$ is the integrated curvatures of the outer raceway which is the equivalent velocity of contact pair.

*2.2.2. Theoretical EHL Model.* The force on an element in the lubricating film in the $x$ direction is shown in Figure 3, assuming that the fluid element is subject to fluid pressure $p$ and shearing stress $\tau$. $u$, $v$, and $w$ are the surface velocities in the $x$, $y$, and $z$ directions, respectively. The velocity $u$ is the main velocity component, followed by $v$. $z$ is along the thickness direction of the film, and its value is much smaller than $x$ or $y$. Therefore, the $dxdz$ surface has no viscous shear stress in the $x$ direction.

The one-dimensional fluid Reynolds equation based on the Herschel–Bulkley grease constitutive model is

$$\frac{n}{2n+1}\cdot\left(\frac{1}{2}\right)^{n+1/n}\left\{\frac{d}{dx}\left[\rho h^{2n+1/n}\left(\frac{1}{\phi}\right)^{1/n}\left(1+\frac{n}{n+1}\frac{2\tau_s}{(\partial p/\partial x)h}\right)\cdot\left(1-\frac{2\tau_s}{(\partial p/\partial x)h}\right)^{n+1/n}\right]\right\}=U\frac{d\rho h}{dx}, \tag{5}$$

where $n$ is the rheological index of the lubricant, $h$ is the film thickness, and $\phi$ is the plastic viscosity, and $\tau_s$ is the yield shear stress of grease.

The film thickness consists of two parts: rigid displacement and elastic deformation. When the roller and raceway are in contact, the film thickness equation at point $x$ is

$$h(x)=h_0+\frac{x^2}{2R}+v(x), \tag{6}$$

where $h_0$ is the film thickness at the center if the surfaces are assumed to be rigid, $R$ is the integrated radius of curvature, and $v(x)$ the elastic deformation displacement due to pressure deformation.

The schematic of the line-load deformation is shown in Figure 4. According to the basic theory of elastic mechanics, the elastic displacement of each node on the surface of the contact body is obtained as follows:

$$v(x)=-\frac{2}{\pi E}\int_{s_1}^{s_2}p(s)\ln\ (s-x)^2ds+c, \tag{7}$$

where $p(x)$ is the line-contact load distribution function; $p(s)ds$ is the distance between an arbitrary line load and the coordinate origin; $s_1$ and $s_2$ are the starting and ending coordinates of load $p(x)$, respectively; and $c$ is an undetermined constant.

The equation of viscosity varying with pressure and temperature is

$$\phi=\phi_0\exp\left\{(ln\,\phi_0+9.67)\left[-1+\left(1+\frac{p}{p_0}\right)^z\times\left(\frac{T-138}{T_0-138}\right)^{-1.1}\right]\right\}, \tag{8}$$

where $T$ is the grease temperature and $T_0$ is the initial temperature, generally taken to be 303 K.

The density equation is obtained based on the experimental curve. The density-pressure relationship [27] is given by

$$\rho=\rho_0\left[1+\frac{0.6p}{1+1.7p}\right], \tag{9}$$

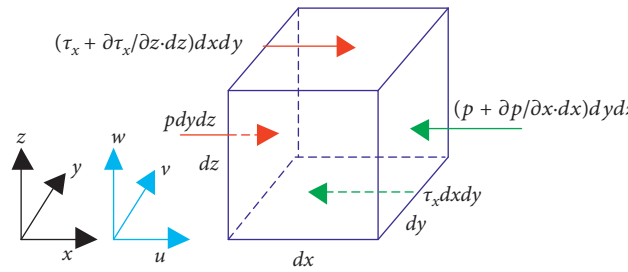


Figure 3: Equilibrium of an element.

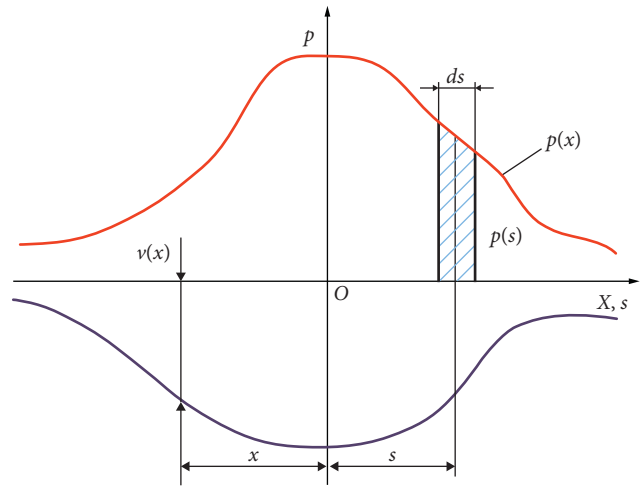


Figure 4: Schematic of line-load deformation.

where $\rho_0$ is the density of the lubricant when the pressure is zero.

Heat loss depends mainly on the heat conduction, the temperature is an important factor for the high-speed lubrication, and thus the energy equation is

$$\rho c_p u\frac{\partial T}{\partial x}=k\frac{\partial^2 T}{\partial z^2}-\frac{T}{\rho}\frac{\partial\rho}{\partial T}\left(u\frac{\partial p}{\partial x}\right)+\phi\left(\frac{\partial u}{\partial z}\right)^2, \tag{10}$$

where $c_p$ is the specific heat capacity at constant pressure and $k$ is the heat-transfer coefficient.

*2.2.3. Load-Balance Equation.* Assuming that the contact load of the rollers is uniformly distributed in the axle box bearing, and based on the principle of line-contact grease lubrication, the load-balance equation is established based on the slicing method. The principle of the slicing method is the following: (1) to cut the bearing roller along the generatrix direction into the $N$ unit pieces; (2) to analyze the film pressure and thickness of each slice unit; and (3) to obtain the bearing film pressure and thickness distribution. A slicing method-specific diagram of a bearing roller is shown in Figure 5. It is convenient and effective to translate the three-dimensional complex EHL problem into a line-contact EHL problem through the slicing method. Thereby, to a great extent, the computational complexity is simplified, and the solution efficiency is improved.

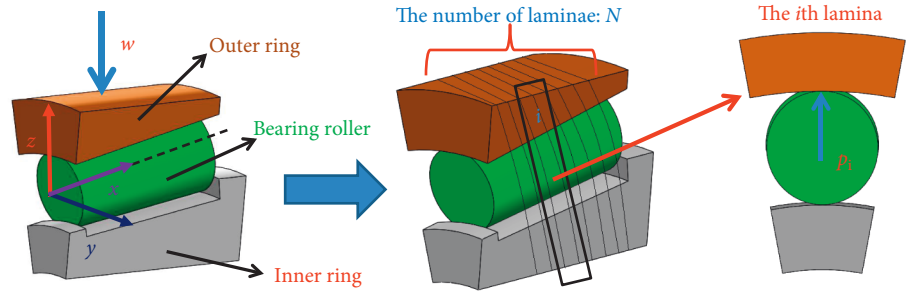


Figure 5: Schematic of line-load deformation.

Solving the line-contact EHL problem is carried out under certain loading conditions. The lubrication film pressure must meet the load-balance condition. Thus, the load-balance equation is

$$w - \int_{x_0}^{x_e} p(s)ds = 0, \tag{11}$$

where $w$ is the external excitation of the bearing rollers; for the line contact, $w$ is the linear load.

Equation (11) is nondimensionalized and discretized, and thus, the discretized load equation is

$$\Delta X \sum_{i=1}^{N} \frac{P_i + P_{i+1}}{2} = \frac{\pi}{2}, \tag{12}$$

where $p_i$ is the linear contact load of the $i$th lamina of a single roller bearing.

*2.2.4. Boundary Equation.* The tangential velocity equation of the lower and upper surfaces of the bearing roller is

$$\begin{cases} u_1 = 0.5 \times (2 + s) \times U, \\ u_2 = 0.5 \times (2 - s) \times U, \end{cases} \tag{13}$$

where $u_1$ and $u_2$ are the tangential velocity equations of the lower and upper surfaces of the bearing, respectively, and $s$ is the slide/roll ratio of the bearing.

Because the contact body is in a moving state, the calculation of temperature on the contact surface can be reduced to the heat conduction problem with a moving heat source in semi-infinite space. The boundary equation of the two contact surfaces is

$$\begin{cases} T(x,0) = \dfrac{k}{\sqrt{\pi\rho_1 c_1 k_1 u_1}} \displaystyle\int_{-\infty}^{x} \left.\frac{\partial T}{\partial z}\right|_{x,0} \frac{ds}{\sqrt{x-s}} + T_0, \\ T(x,h) = \dfrac{k}{\sqrt{\pi\rho_2 c_2 k_2 u_2}} \displaystyle\int_{-\infty}^{x} \left.\frac{\partial T}{\partial z}\right|_{x,h} \frac{ds}{\sqrt{x-s}} + T_0, \end{cases} \tag{14}$$

where $k_1$ and $k_2$ are the thermal conductivities of the two contact surface materials, respectively, $c_1$ and $c_2$ their specific heat capacities, respectively, and $\rho_1$ and $\rho_2$ their densities, respectively.

*2.2.5. Numerical Analysis.* For the sake of improving the stability of the calculation, it is necessary to nondimensionalize the thermal EHL equation. The calculated area is $X_{in} = -4$ and $X_{out} = 1$. The discretized equations are obtained by the finite-difference method, and the relaxation iteration of film pressure and thickness is then solved by the multigrid method [28, 29]. Finally, the numerical solution is obtained on the densest grid. The multigrid method is divided into six layers, and the bearing roller is divided into 30 pieces along the generatrix direction. The calculation flowchart of the thermal EHL equation is shown in Figure 6.

*2.3. Structural Parameters.* Based on an engineering example, the vehicle axle box bearing dynamic load distribution and thermal THL characteristics were analyzed. A axle box bearing was used here as an instance. The structure parameters of such axle box bearing and wheelset/track system are illustrated in Table 1. The parameters of the bearing lubricating grease are shown in Table 2.

*2.4. Track Irregularity.* The ballastless track spectrum is adopted as the sample input for track irregularity. Ballastless track irregularity of high-speed railway is fitted by power function piecewise, and the track spectrum of each wavelength section is expressed uniformly [26]:

$$S(f) = \frac{A}{f^n}, \tag{15}$$

where the unit of $S(f)$ is $mm^2/(1/m)$, $f$ is the spatial frequency (1/m), and $A$ and $n$ are fitting coefficients.

According to the power spectrum of random track irregularity, the amplitude and phase of the spectrum are acquired by the periodogram method, and then the time-domain simulation sample of track irregularity is obtained by an inverse fast Fourier transform (IFFT). According to the numerical simulation method of a track spectrum, the vertical track irregularity sample is shown in Figure 7.

## 3. Results

The speed and integrated curvature of the contact pair for axle box bearings are shown in Figure 8. As the diameter of the roller increases, the integrated curvature of the outer and inner raceway increases and that of outer raceway is bigger than the inner raceway.

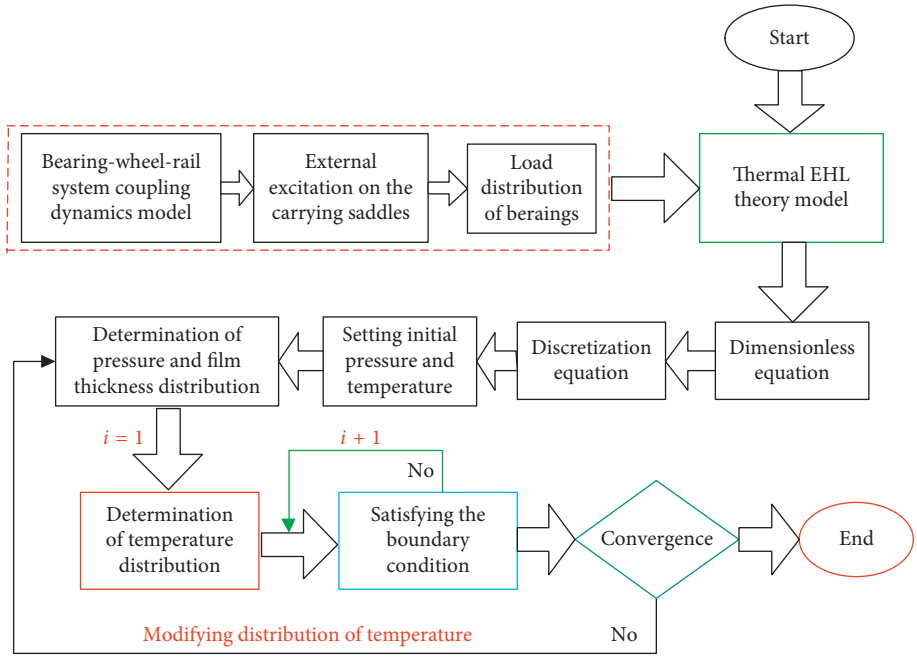


Figure 6: Calculation flowchart of the thermal EHL equation.

Table 1: Structural parameters of the axle box bearing and wheelset/track system.

| Axle box bearing | | Wheelset/track system | |
|---|---|---|---|
| Average diameter of roller (mm)$D_w$ | 25.715 | Mass of the rail with unit length (kg/m)$m_r$ | 60.64 |
| Number of roller | 22 | Rail's elasticity modulus (N/m$^2$)$E$ | 2.059$e$11 |
| Equivalent contact length (mm)$l$ | 57 | Rail's cross-sectional inertia (m$^4$)$I$ | 3.217$e$−5 |
| Outer ring contact angle ($\alpha_e$) | 9°59′6″ | Stiffness of the rail pads (N/m)$k_p$ | 6.5$e$7 |
| Inner ring contact angle ($\alpha_i$) | 7°52′ | Damping of the rail pad (N·s/m)$c_p$ | 7.5$e$4 |
| Flange contact angle ($\alpha_f$) | 81°4′ | Total number of orders NM | 156 |
| Mass of the bearing outer ring (kg) $m_b$ | 15.2 | Mass of the adapter (kg) $m_c$ | 77.2 |

Table 2: Parameters of bearing lubricating grease.

| | |
|---|---|
| Speed of bearing inner ring (r/min) | 795 |
| Synthetical elastic modulus (Pa) | 2.21$e$11 |
| Rheological index ($n$) | 0.98 |
| Initial temperature (°C) | 30 |
| Initial kinematic viscosity (Pa·s) | 0.15 |
| Grease density (kg/m$^3$) | 890 |
| Heat transfer coefficient of lubricant grease (W/m·°C) | 0.14 |
| Heat transfer coefficient of bearing (W/m·°C) | 46 |
| Specific heat capacity of lubricating grease (J·kg$^{-1}$·K$^{-1}$) | 2000 |
| Specific heat capacity of bearing (J·kg$^{-1}$·K$^{-1}$) | 470 |
| Initial density of bearing (kg/m$^3$) | 7850 |

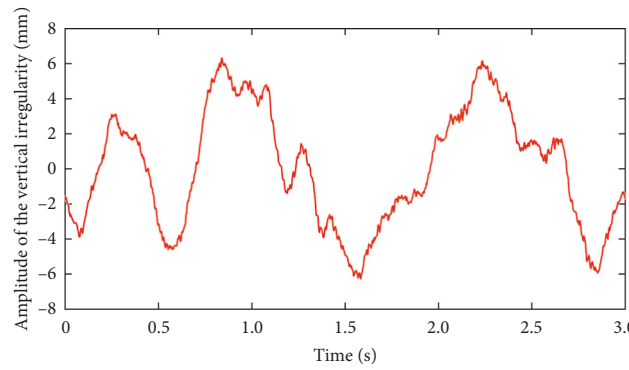


Figure 7: Vertical track irregularity sample.

*3.1. Bearing Load.* According to the bearing-wheel-rail coupled dynamics model and the load under the carrying saddles, the loading-time course of the rollers of the axle box bearing can be obtained. The loading-time course of the maximum load roller of the axle box bearings are shown in Figure 9.

*3.2. Film Distribution.* Figure 10 shows the distribution of the film thickness and pressure in the contact area between the inner/outer raceway and roller. Figure 11 presents the distribution of film pressure and thickness along the roller generatrix under inner and outer contact conditions.

As illustrated in Figure 11, the maximum film pressure in the surface contact center of the inner and outer raceway contacts is 0.778 and 0.690 GPa, respectively, and the minimum film thicknesses are 0.561 and 0.613 $\mu$m, respectively. Figures 11(a) and 11(b) show that the film thicknesses of the roller in the center zone is reduced by 8.5%

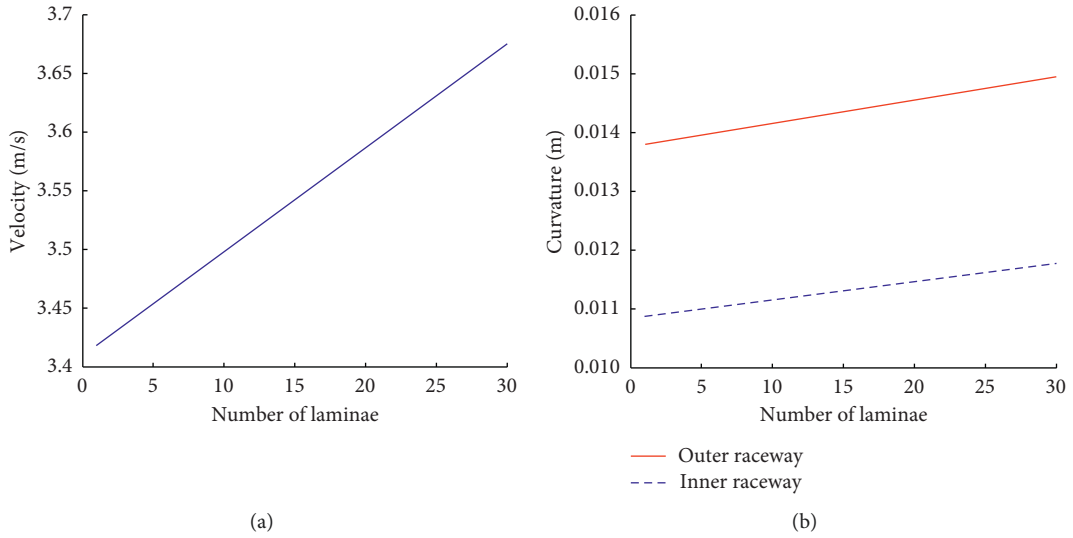


Figure 8: Contact parameters of bearings: (a) speed and (b) integrated curvature of contact pair.

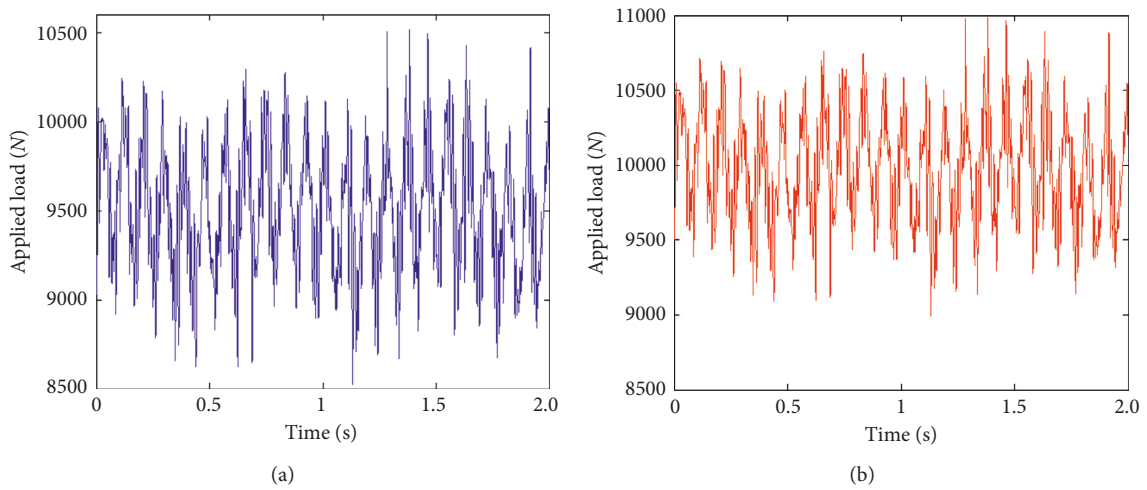


Figure 9: Loading-time course of the maximum load roller: (a) left- and (b) right-hand axle box bearings.

from the large to small end along the generatrix direction, and the film pressure is increased by 4%.

*3.3. Influence of Working Conditions.* In Figures 12 and 13, the change rule of film pressure and thickness is gained under different loads and contact-load speeds, respectively.

The maximum film pressure rises with the increasing load, presenting line variety, and a pressure-change rate of 1.6 MPa/kN, as shown in Figure 12(c). Figure 12(d) shows that the minimum and mean film thicknesses both decrease with an increasing load and also presents line variety, but the amplitude variation is not significant.

Figure 13(c) indicates that the maximum contact pressure decreases with the increasing contact-pair speed, while the pressure is almost unchanged. Figure 13(d) shows that the minimum and mean film thicknesses increase with the increasing contact-pair speed, presenting line variety, and the thickness change rate is 0.12 $\mu$m·s/m.

*3.4. Thermal Effects on EHL.* The lubrication condition of the roller small end is worse than that of the roller large end. So the film pressure and thickness of the cross section of the roller small end was analyzed. Figure 14 shows the results of comparing isothermal and thermal EHL lubrication based on the lubrication model.

Figure 14(a) shows that the pressure-spike amplitude is 0.778 GPa and the pressure of the contact center is 0.777 GPa under the thermal EHL condition. Under the isothermal EHL condition, the pressure-spike amplitude is 1.092 GPa, and the pressure of the contact center is 0.799 GPa. The pressure-spike amplitude increases by 36.65% more than the pressure of the contact center. Figure 14(b) shows that the minimum film thickness is 0.561 $\mu$m; mean film thickness in the contact region of [−1, 1] is 0.660 $\mu$m under the thermal EHL condition. Under the isothermal EHL condition, the minimum film thickness is 0.589 $\mu$m; mean film thickness in the contact region of [−1, 1] is 0.764 $\mu$m.

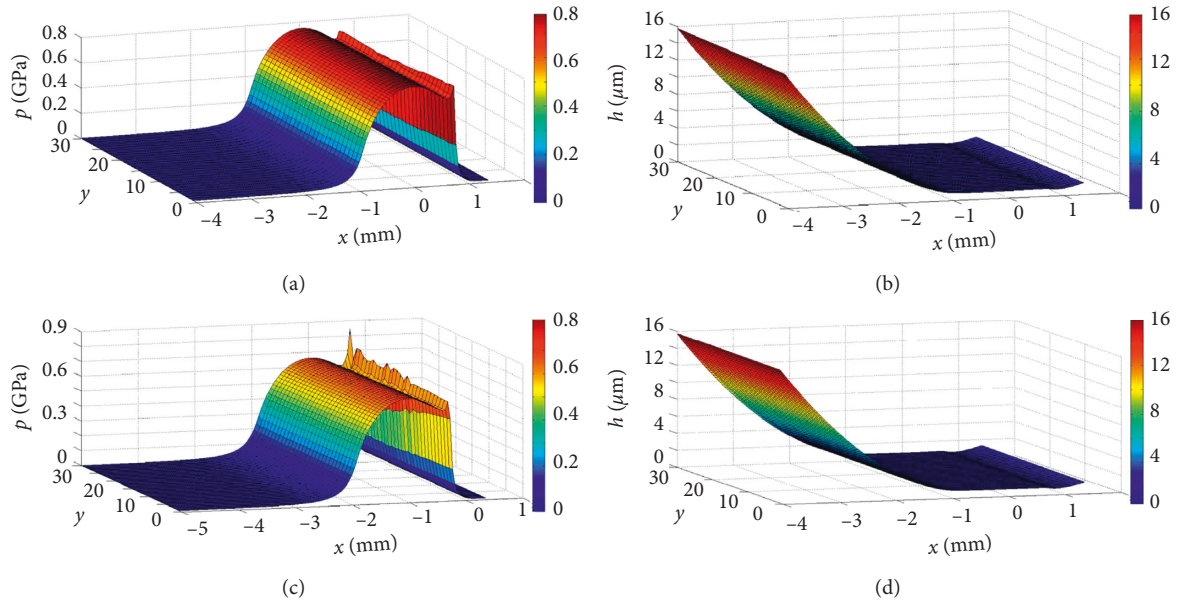


Figure 10: Distribution of film pressure and thickness under the outer and inner raceway contact conditions: distribution of (a) film pressure of the inner raceway; (b) film thickness of the inner raceway; (c) film pressure of the outer raceway; (d) film thickness of the outer raceway.

The film pressure and thickness are sensitive to the contact-pair speed. Figure 15 presents the pressure and thickness distributions of the isothermal and thermal EHL film under different contact-pair speeds.

Compared to those under isothermal EHL, the film pressure and thickness under thermal EHL are significantly different. With the increasing contact-pair speed, the differences in pressure and thickness between thermal and isothermal EHL increase rapidly. The film thickness and pressure-spike amplitude of thermal EHL are very sensitive to the contact-pair speed. Figure 15(d) shows that the pressure-spike amplitude is 1.187 GPa and increases by 52.8% more than it does under isothermal EHL, when the contact-pair speed is 4 m/s. Figure 15(g) shows that the film thickness of thermal EHL in the central contact zone is 0.730 $\mu$m and is reduced by 19.7% compared to that of isothermal EHL.

## 4. Discussion

The axle box bearing is the key load-carrying component of a vehicle wheel system, and its dynamics and lubrication parameters directly affect the safe operation of train. In this paper, we have established a dynamics model of the bearing-wheel-rail coupled dynamics model that considers nonlinear contact bearing load, and then we have obtained the load distribution and load history of the bearing rollers, which provide the boundary conditions for dynamic characteristic analysis and design of the lubrication of axle box bearings. At the same time, considering the scale effect of the roller and raceway, we have established the thermal EHL theory model based on bearing-roller slicing theory, which provides a theoretical foundation for the lubrication system design of vehicle axle box bearings.

The scale effect of roller and raceway cannot be ignored, in term of thermal EHL characteristics of axle box bearings. In Figure 10, compared to the inner-raceway contact, the pressure in the surface contact center of the outer raceway contact is smaller, and the film thickness is larger. Therefore, the lubrication condition of the outer raceway is better than that of the inner raceway. In Figures 11(c) and 11(d), the film pressure of the central section of the roller increases gradually approaching the contact center, and there is the pressure-spike amplitude in the exit zone. The film thickness of the lubricant in the contact zone changes gently, but it clearly shows necking phenomena at the exit region. Bruyere et al. obtained similar results by establishing the finite-line-contact EHL model [17–19]. At the same time, the EHL model of Mihailidis et al. [18] does not consider the scale effect of the roller raceway, so the film pressure and thickness along the direction of the roller generatrix is the same. Najjari and Guilbault [19] established an EHL model considering the boundary effect of the roller (roller-edge-curvature change), and the film pressure and thickness of the roller intermediate region is also unchanged along the roller generatrix direction, while the film pressure increases sharply in the edge of the roller. However, we see from Figures 11(a) and 11(b), along the generatrix direction, that the film thickness of the roller is decreased by 8.5% from the large end to the small end, and the film pressure increases by 4%. The maximum film pressure and minimum film thickness of tapered roller bearings is at the small end bearing roller, so roller lubrication of the small end is worse. The scale effect of the roller and raceway lead to the changing of the pressure and film thickness in the middle part of the roller. Therefore, in the study of the finite-line-contact EHL model, the scale effect of the roller and raceway is the key to accurately obtain the pressure and thickness distributions.

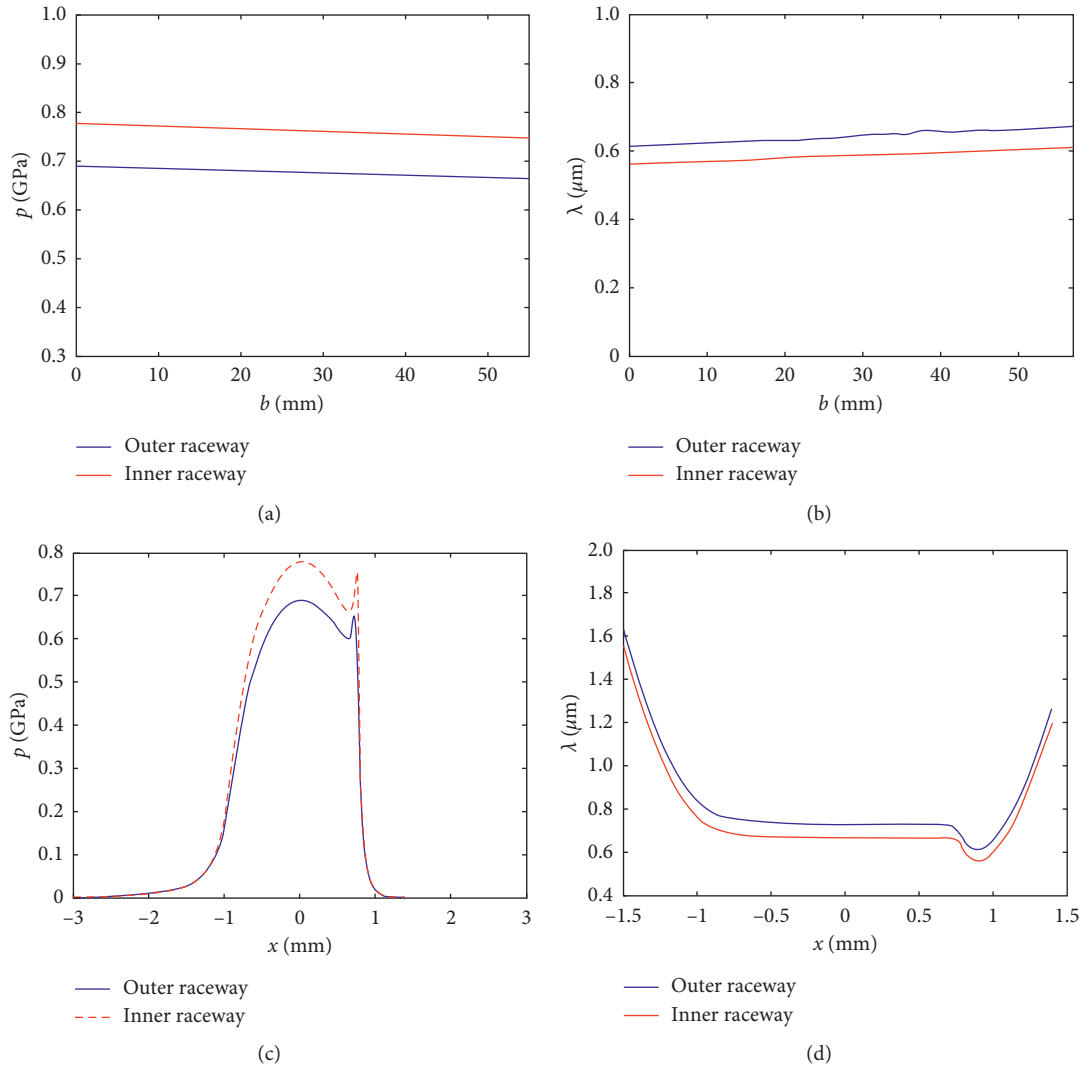


Figure 11: Distribution of film pressure and thickness along the roller generatrix under inner and outer contact conditions: distribution of (a) film pressure along the surface generatrices; (b) film thickness along the surface generatrices; (c) film pressure at the cross section; (d) film thickness at the cross section.

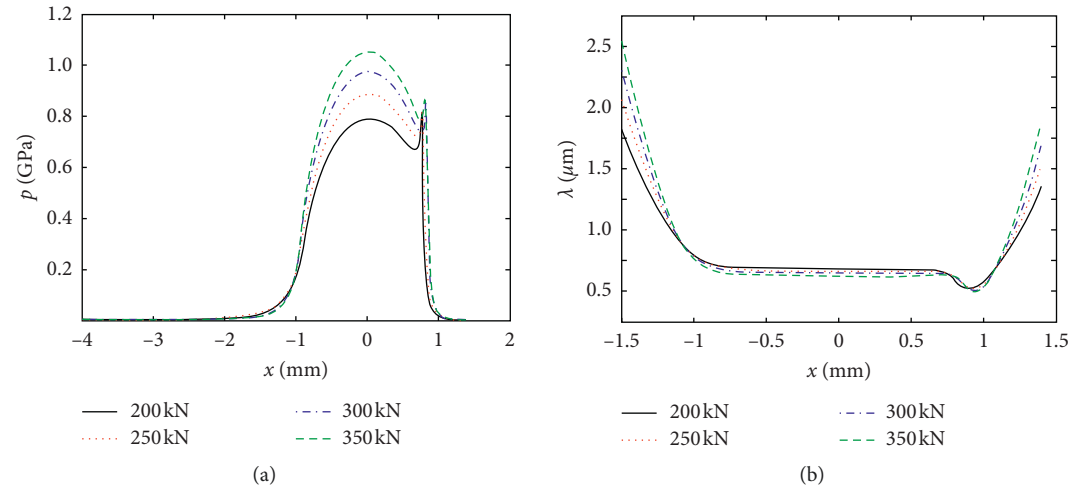


Figure 12: Continued.

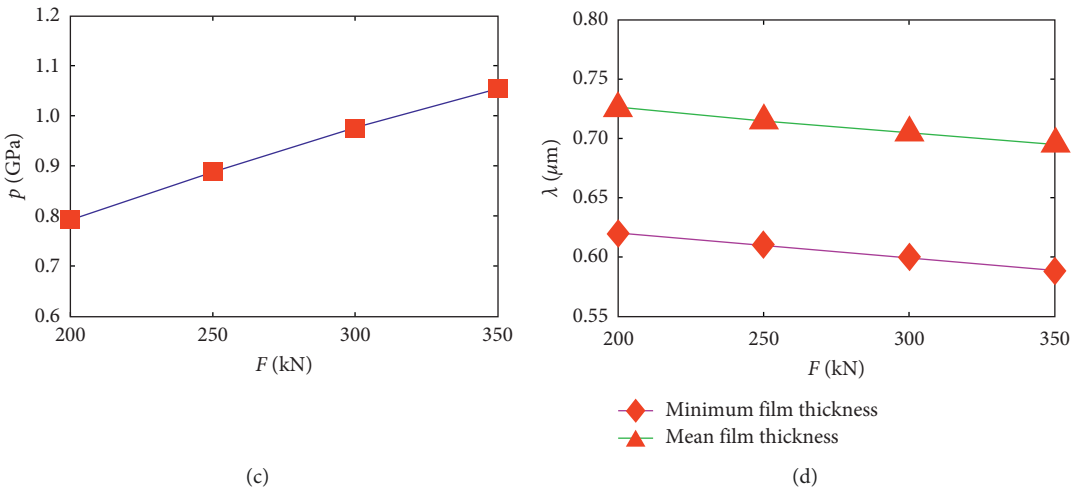


Figure 12: Comparison of lubrication characteristics under different loads: (a) film pressure distribution; (b) film thickness distribution; (c) maximum film pressure; (d) minimum film thickness and mean film thickness.

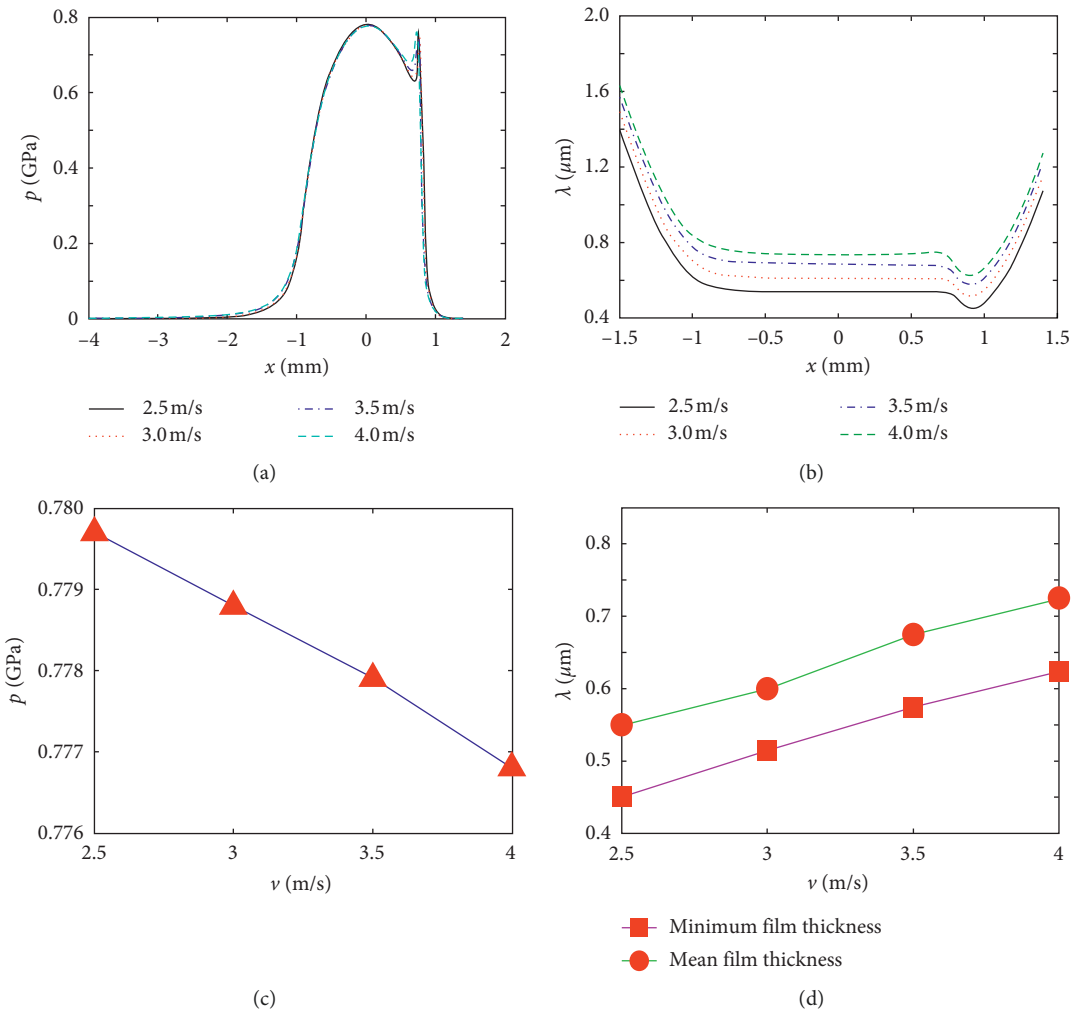


Figure 13: Comparison of lubrication characteristics under different contact-pair speeds: (a) film pressure distribution; (b) film thickness distribution; (c) maximum film pressure; (d) minimum and mean film thickness.

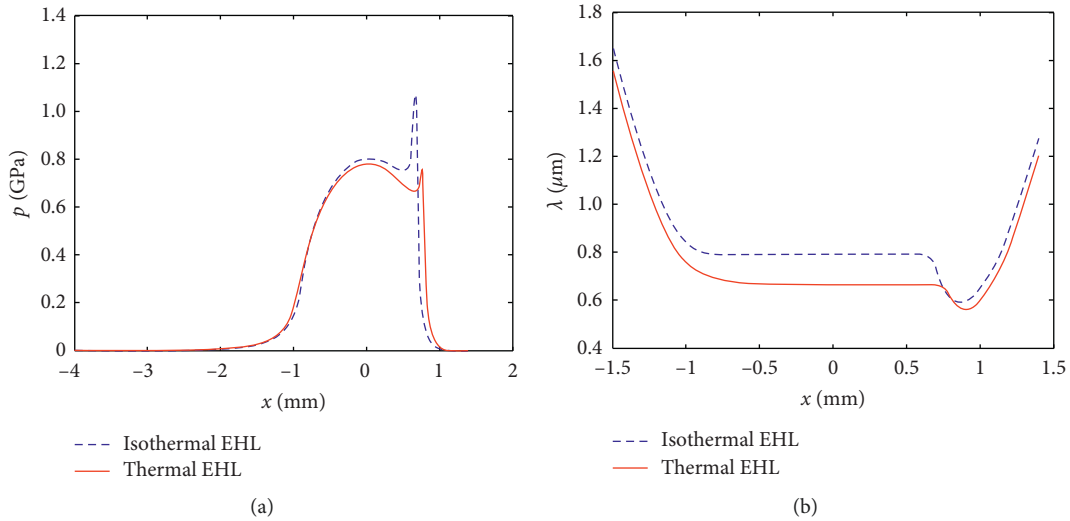


Figure 14: Comparison of the results under isothermal and thermal EHL lubrication: (a) film pressure; (b) film thickness distribution.

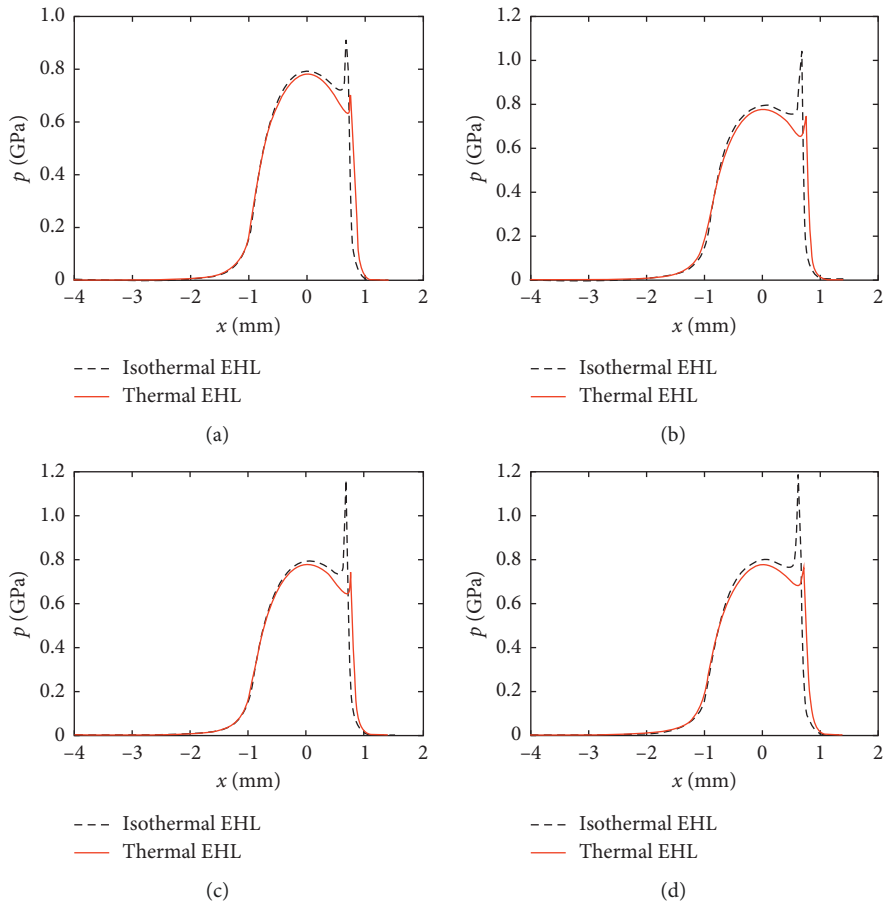


Figure 15: Continued.

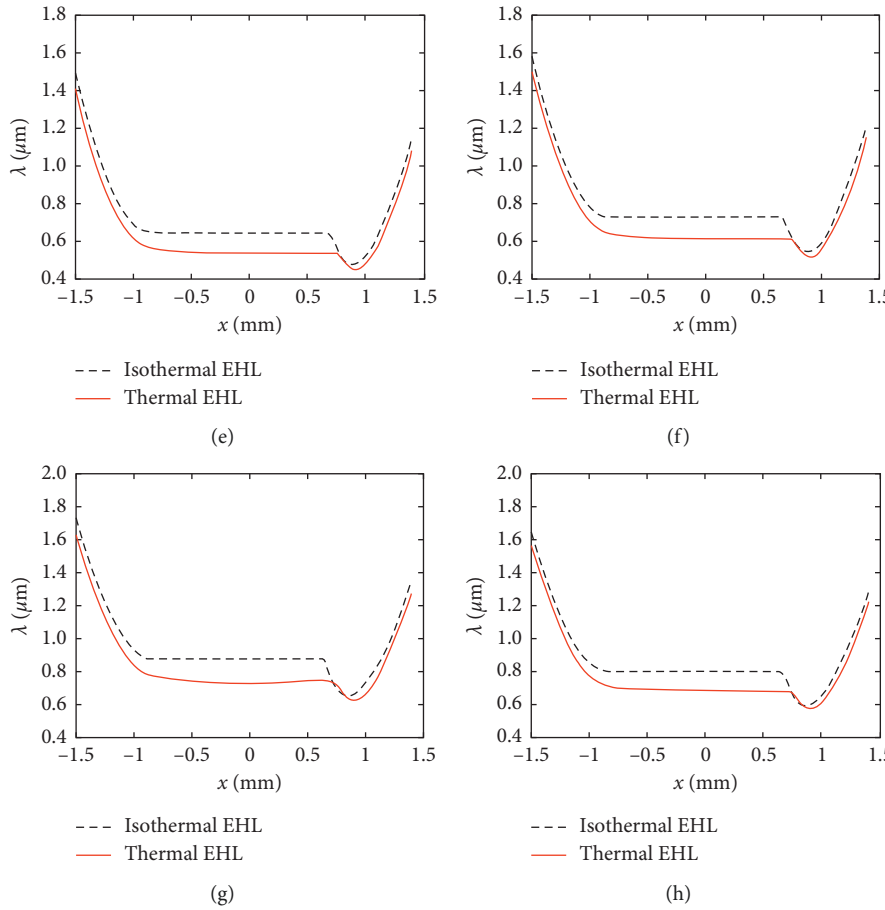


Figure 15: Comparison of film pressure distribution results under isothermal and thermal EHL lubrication at the velocity of (a) 2.5 m/s, (b) 3.0 m/s, (c) 3.5 m/s, and (d) 4.0 m/s and film thickness distribution-comparison of results under the isothermal and thermal EHL lubrication at the velocity of (e) 2.5 m/s, (f) 3.0 m/s, (g) 3.5 m/s, and (h) 4.0 m/s.

The lubrication characteristics of axle box bearings have different sensitivities to load and speed. In Figure 12, under a certain contact velocity, the film pressure is more sensitive to the load than the film thickness, and the pressure-change rate is 1.6 MPa/kN. In Figure 13, under a certain load condition, the film thickness is more sensitive to the velocity of the contact pair than the film pressure, and the film thickness change rate is 0.12 $\mu$m·s/m. The study of Hili et al. [16], based on experiment, shows that, with the rapid increase of the contact-pair speed, the film thickness of the contact area increases rapidly, which is consistent with the results of this paper regarding the film thickness variation. Therefore, it is necessary to check the film pressure under impact load in order to prevent the plastic deformation caused by high film pressure. At the same time, it is equally necessary to consider the influence of the sharp drop of the contact-pair speed on the film thickness under braking conditions in order to prevent dry grinding of the bearings due to the film thickness being too small.

Temperature has a great influence on film thickness in the EHL model. In Figure 14, the maximum film pressure of the thermal EHL is shown to be reduced by 28.77% more than that of the isothermal EHL, while the pressure of the contact center decreased by 2.67%. These results show that the temperature has little influence on the pressure of the contact center but has a great influence on the formation of the pressure-spike amplitude. Compared to isothermal EHL, the minimum film thickness is reduced by 4.84%, and the mean film thickness is reduced by 13.61%. Wu studied the effect of the thermal and isothermal EHL models on line-contact cam pairs [20], and the results presented in this paper are consistent with Wu's.

Investigating the influence of velocity on thermal EHL analysis showed that, compared to isothermal and thermal EHL, the film pressure and thickness exhibit great differences depending on contact-pair speed. In Figure 15, the film thickness of thermal EHL is always smaller than that of isothermal EHL. Meanwhile, as the contact-pair speed increases, the difference in the film thickness between thermal EHL and isothermal EHL exhibits a larger increase. This finding is consistent with that of Liu's study on the effect of speed on line-contact EHL in gear pairs [21]. Therefore, it is necessary to consider the thermal effects of a lubricant in researching finite-line contact thermal EHL of high-speed axle box bearings. The speed is also the key factor affecting the thermal EHL characteristics.

## 5. Conclusions

This paper has fully considered track irregularities in establishing the bearing-wheel-rail system-coupled dynamics model and obtained the dynamic load history of axle box bearings. The load-balance equation and thermal EHL model were obtained according to the slicing method of bearing rollers. Numerical solution showed that the film pressure of the central section of the roller increases gradually approaching the contact center and that there is the pressure-spike amplitude in the exit zone of 0.778 GPa. The film thickness of the lubricant in the contact zone changes gently, but necking phenomena are clearly shown at the exit region; the minimum film thickness is 0.561 $\mu$m. The lubrication characteristics among the factors affecting the sensitivity analysis showed that the film pressure is sensitive to the load, and the pressure increases with the increasing load. The film thickness is sensitive to the contact-pair speed, and the film thickness decreases with decreasing contact-pair speed. According to the analysis of thermal effects on EHL, the results indicated that the central film thickness under thermal EHL decreased by 13.61% compared to that under isothermal EHL. As the contact-pair speed increases, the thickness difference between thermal and isothermal EHL became larger. Thus, thermal effects should be considered in the EHL model, in order to truly reflect the characteristics of high-speed EHL.

## Data Availability

All data included in this study are available upon request by contacting the corresponding author.

## Conflicts of Interest

The authors declare that they have no conflicts of interest.

## Acknowledgments

This work was supported by the National Key R&D Program of China (no. 2018YFB1306701), National Natural Science Foundation of China (no. 51875076), NSFC-Liaoning United Key Fund (no. U1708255), and Opening Foundation of State Key Laboratory of Shield Machine and Boring Technology (no. SKLST-2018-K04).

## References

[1] B. Dyniewicz and C. I. Bajer, "New feature of the solution of a Timoshenko beam carrying the moving mass particle," *Archives of Mechanics*, vol. 62, no. 5, pp. 327–341, 2010.

[2] J.-Q. Jiang, "Transient responses of Timoshenko beams subject to a moving mass," *Journal of Vibration and Control*, vol. 17, no. 13, pp. 1975–1982, 2011.

[3] T. Mazilu, M. Dumitriu, and C. Tudorache, "On the dynamics of interaction between a moving mass and an infinite one-dimensional elastic structure at the stability limit," *Journal of Sound and Vibration*, vol. 330, no. 15, pp. 3729–3743, 2011.

[4] K. Wang, P. Liu, W. Zhai, C. Huang, Z. Chen, and J. Gao, "Wheel/rail dynamic interaction due to excitation of rail corrugation in high-speed railway," *Science China Technological Sciences*, vol. 58, no. 2, pp. 226–235, 2015.

[5] W. Zhai, J. Gao, P. Liu, and K. Wang, "Reducing rail side wear on heavy-haul railway curves based on wheel–rail dynamic interaction," *Vehicle System Dynamics*, vol. 52, no. 1, pp. 440–454, 2014.

[6] W. Zhai, K. Wang, and C. Cai, "Fundamentals of vehicle-track coupled dynamics," *Vehicle System Dynamics*, vol. 47, no. 11, pp. 1349–1376, 2009, in English.

[7] W. Zhai and X. Sun, "A detailed model for investigating vertical interaction between railway vehicle and track," *Vehicle System Dynamics*, vol. 23, no. 1, pp. 603–615, 1994.

[8] W. Zhai, K. Wei, X. Song, and M. Shao, "Experimental investigation into ground vibrations induced by very high speed trains on a non-ballasted track," *Soil Dynamics and Earthquake Engineering*, vol. 72, pp. 24–36, 2015.

[9] Q. Zhang, Ł. Jankowski, and Z. Duan, "Simultaneous identification of moving masses and structural damage," *Structural and Multidisciplinary Optimization*, vol. 42, no. 6, pp. 907–922, 2010.

[10] L. Liu, Y. Zang, and Y. Chen, "Hydrodynamic analysis of partial film lubrication in the cold rolling process," *International Journal of Advanced Manufacturing Technology*, vol. 54, no. 5–8, pp. 489–493, 2011.

[11] S.-C. Tzeng, W.-P. Ma, C.-W. Lin, W.-Y. Jywe, C.-H. Liu, and Y.-C. Wang, "Experimental investigation of lubrication and cooling effects of high-speed rotating machines," *International Journal of Advanced Manufacturing Technology*, vol. 35, no. 3-4, pp. 394–399, 2007.

[12] P. Yang and S. Wen, "A generalized reynolds equation for non-newtonian thermal elastohydrodynamic lubrication," *Journal of Tribology*, vol. 112, no. 4, pp. 631–636, 1990.

[13] L. Rong-Tsong and H. Chao-Ho, "A fast method for the analysis of thermal-elastohydrodynamic lubrication of rolling/sliding line contacts," *Wear*, vol. 166, no. 1, pp. 107–117, 1993.

[14] W. Habchi, *Coupling Strategies for Finite Element Modeling of Thermal Elastohydrodynamic Lubrication Problems*, Wiley, Hoboken, NJ, USA, 2016.

[15] W. Habchi and J. S. Issa, "An exact and general model order reduction technique for the finite element solution of elastohydrodynamic lubrication problems," *Journal of Tribology*, vol. 139, no. 5, article 051501, 2016.

[16] J. Hili, A. V. Olver, S. Edwards, and L. Jacobs, "Experimental investigation of elastohydrodynamic (EHD) film thickness behavior at high speeds," *Tribology Transactions*, vol. 53, no. 5, pp. 658–666, 2010.

[17] V. Bruyere, N. Fillot, G. E. Morales-Espejel, and P. Vergne, "Computational fluid dynamics and full elasticity model for sliding line thermal elastohydrodynamic contacts," *Tribology International*, vol. 46, no. 1, pp. 3–13, 2012.

[18] A. Mihailidis, K. Agouridas, and K. Panagiotidis, "Non-newtonian starved thermal-elasto hydrodynamic lubrication of finite line contacts," *Tribology Transactions*, vol. 56, no. 1, pp. 88–100, 2013.

[19] M. Najjari and R. Guilbault, "Edge contact effect on thermal elastohydrodynamic lubrication of finite contact lines," *Tribology International*, vol. 71, pp. 50–61, 2014.

[20] W. Wu, J. Wang, and C. H. Venner, "Thermal elastohydrodynamic lubrication of an optimized cam–tappet pair in smooth contact," *Journal of tribology–Transactions of the ASME*, vol. 138, no. 2, article 021501, 2015.

[21] M. Liu, C. Zhu, H. Liu, and C. Wu, "Parametric studies of lubrication performance of a helical gear pair with non-

Newtonian fluids," *Journal of Mechanical Science and Technology*, vol. 30, no. 1, pp. 317–326, 2016.

[22] M. Liu, C. Zhu, H. Liu, H. Ding, and Z. Sun, "Effects of working conditions on TEHL performance of a helical gear pair with non-newtonian fluids," *Journal of Tribology*, vol. 136, no. 2, article 021502, 2014.

[23] J. Huo, H. Wu, D. Zhu, W. Sun, L. Wang, and J. Dong, "The rigid–flexible coupling dynamic model and response analysis of bearing–wheel–rail system under track irregularity," *ARCHIVE Proceedings of the Institution of Mechanical Engineers Part C Journal of Mechanical Engineering Science*, vol. 203–210, pp. 1989–1996, 2017.

[24] X. Shi and L. Wang, "TEHL analysis of high-speed and heavy-load roller bearing with quasi-dynamic characteristics," *Chinese Journal of Aeronautics*, vol. 28, no. 4, pp. 1296–1304, 2015.

[25] X. Zhang, Q. Han, Z. Peng, and F. Chu, "A comprehensive dynamic model to investigate the stability problems of the rotor-bearing system due to multiple excitations," *Mechanical Systems and Signal Processing*, vol. 70-71, pp. 1171–1192, 2016.

[26] W. M. Zhai, *Vehicle-Track Coupled Dynamics*, Vol. 1, Science Press, Beijing, China, 2015.

[27] D. Zhu and S.-Z. Wen, "A full numerical solution for the thermoelastohydrodynamic problem in elliptical contacts," *Journal of Tribology*, vol. 106, no. 2, pp. 246–254, 1984, in English.

[28] A. Brandt and A. A. Lubrecht, "Multilevel matrix multiplication and fast solution of integral equations," *Journal of Computational Physics*, vol. 90, no. 2, pp. 348–370, 1990.

[29] C. H. Venner, "Higher-order multilevel solvers for the EHL line and point contact problem," *Journal of Tribology*, vol. 116, no. 4, pp. 741–750, 1994.